SUPPLEMENTARY INFORMATION

Supplementary Material and Methods

Restriction fragment length polymorphism analysis

To confirm m.14674T>C mutation, the 187-bp PCR fragment with the mismatched and reverse primers was digested by *Bcl I*. If the fragment had m.14674T>C mutation, cleaved fragments of 167 and 20 bps would be obtained. To identify m.14674T>G mutation, we amplified the 541-bp PCR fragment and performed *Nla III* digestion. In the absence of this mutation, cleaved fragments of 408 and 133 bps would be detected; however, if the fragment had m.14674T>G mutation, cleaved fragments of 408 bp would be divided into 242- and 166-bp fragments. Each fragment was detected on a 4% agarose gel and visualized with ethidium bromide under UV light.

Quantification of $tRNA^{Glu}$

Northern blot analysis was performed using total RNA extracted from muscle specimens of patients 2 and 4, from whom a sufficient quantity of RNA was obtained, and from muscle specimens of normal infants (normal controls). Samples of total RNA

were electrophoresed through denaturing 10% polyacrylamide containing 7 M urea. RNA was blotted on a nylon membrane and fixed by UV irradiation. Northern hybridization was then performed using DNA probe specific for mitochondrial tRNA-glutamate ($tRNA^{Glu}$): 5′-ATTCTCGCACGGACTACAACCACGACCAAT-3′ labeled at the 5′ terminus with [γ-^{32}P]ATP (110 TBq/mmol; GE Healthcare Bio-Science, Buckinghamshire, UK). The $tRNA^{Glu}$ amounts were normalized by the amount of mitochondrial tRNA-Leu (UUR) (a probe specific for mitochondrial tRNA-Leu (UUR), 5′-TGTTAAGAAGAGGAATTGAACCTCTGACTG-3′ was used) and nuclear-encoded 5S ribosomal RNA (a probe specific for 5S ribosomal RNA, 5′-GGGTGGTATGGCCGTAGAC-3′ complementary to the 3′ region was used). The DNA probes were labeled at the 5′ terminus with [γ-^{32}P]ATP and T4 polynucleotide kinase (Toyobo, Osaka, Japan). RNAs were quantified by exposing the membrane to an imaging plate on which the radioactivity levels of the bands were measured using a BAS 1000 bioimaging analyzer (Fuji Photo Film, Tokyo, Japan).

Acid polyacrylamide gel electrophoresis analysis

Total RNA samples extracted from cybrids derived from fibroblasts of patient 6

and human osteosarcoma 143B cells (normal control) were prepared under acidic conditions in a cold room and then dissolved in 0.1 M NaOAc (pH 5.0) according to the literature to prevent deacylation [26]. A portion of RNA samples was incubated in a buffer containing 50 mM Tris-HCl (pH 9.5) for complete deacylation of tRNA samples. The same amount of total RNA containing aminoacyl-tRNAs or forcibly deacylated tRNAs in an acid-loading solution were electrophoresed to separate aminoacyl-$tRNA^{Glu}$ and uncharged $tRNA^{Glu}$. RNA was then analyzed by Northern hybridization using the probe specific for mitochondrial $tRNA^{Glu}$:

5′-ATTCTCGCACGGACTACAACCACGACCAAT-3′ labeled at the 5′ terminus with [γ-^{32}P]ATP. The DNA probes were labeled at the 5′ terminus with [γ-^{32}P]ATP and T4 polynucleotide kinase. RNAs were quantified by exposing the membrane to an imaging plate on which the radioactivity levels of the bands were measured using a BAS 1000 bioimaging analyzer.

Supporting Information

Matsushima et al. 10.1073/pnas.1008924107

SI Text

SI Materials and Methods. ***Preparation of inducible plasmids expressing cMyc-Lon and the Lon S880A mutant.*** The plasmid pMt/Lon/Hy, in which Lon is regulated by the metallothionein promoter, was constructed as follows: a fragment of *Drosophila* Lon cDNA was amplified by PCR using as 5′-primer 5′- GGGCTCGAGTGCGAGTGGATATTGCTTTC -3′ and as 3′-primer 5′- GCGCACTAGTATTACAAGTCTTCTTCAGAAATAAGCTTTTGAGAATAAGGCCACGTCTC -3′. The PCR fragment was cleaved by XhoI and SpeI and subcloned.

pMt/S880A/Hy was constructed from pMt/Lon/Hy by site directed mutagenesis using the following pair of primers: 5′-AGATGGCCCCGCTGCGGGCATC -3′ and 5′- GATGCCCGCAGCGGGGCCATCT -3′.

Detection of carbonylated proteins. The OxyBlot procedure (Millipore) was used to perform immunoblot detection of oxidatively modified proteins by the generation of carbonyl groups. Ten micrograms of protein were used for each reaction. Carbonyl groups in mitochondrial protein samples (10 μg) were derivatized to 2,4-dinitrophenylhydrazone (DNP-hydrazone) by reaction with 2,4-dinitrophenylhydrazine. Carbonylated proteins were detected by immunoblot analysis using an anti-DNP antibody.

Indirect immunofluorescence. Indirect immunofluorescence was performed as described (1) with anti-c-Myc monoclonal antibody (Sigma) and Alexa Fluor 488 anti-mouse IgG (Molecular Probes).

Preparation of inducible plasmids expressing Lon, TFAM, and Lon-Targeted RNAi. The plasmid pMt/Lon/Hy, in which Lon is regulated by the metallothionein promoter, was constructed as follows: a fragment of *Drosophila* Lon cDNA was amplified by PCR using as 5′-primer 5′- GGGCTCGAGTGCGAGTGGATATTGCTTTC -3′ and as 3′-primer 5′- GCGCACTAGTCTAAGAATAAGGCCACGTCTC -3′. The PCR fragment was cleaved by XhoI and SpeI and subcloned. The plasmid pMt/TFAM/Hy was as described previously (2). The plasmid pMt/invLon/Hy carries an inverted repeat of a nucleotide sequence from *Lon* cDNA that is transcribed from the metallothionein promoter. The insert in pMt/invLon/Hy was generated from two PCR-amplified fragments of *Lon* cDNA. One fragment has terminal XhoI and EcoRI sites and was prepared using the following pair of primers: 5′- GCGCCTCGAGACTAGTGGGATGATTCCAACGGGGAT -3′ (forward) and 5′- GCGCGAATTCGGGATCGATTCCGCTTGATCAGTGCTTTG -3′(reverse). A second fragment has terminal SpeI and EcoRI sites and was prepared using the primers 5′- GCGCCTCGAGACTAGTGGGATGATTCCAACGGGGAT -3′ (forward) and 5′- GCGCGAATTCAAAAAGCTTTCCGCTTGATCAGTGCTTTG -3′ (reverse). The two PCR products were ligated and cloned into the pMt/Hy vector cleaved with XhoI and SpeI.

1. Goto A, Matsushima Y, Kadowaki T, Kitagawa Y (2001) *Drosophila* mitochondrial transcription factor A (d-TFAM) is dispensable for the transcription of mitochondrial DNA in Kc167 cells *Biochem J* 354:243–248.

2. Matsushima Y, Garesse R, Kaguni LS (2004) *Drosophila* mitochondrial transcription factor B2 regulates mitochondrial DNA copy number and transcription in schneider cells. *J Biol Chem* 279:26900–26905

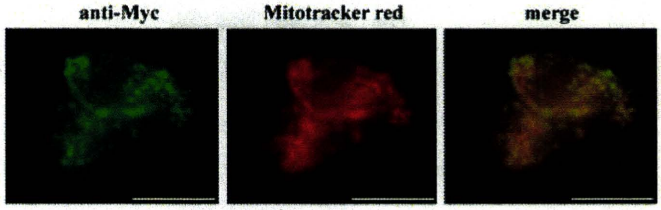

Fig. S1. Overexpression of *Drosophila* Lon in Schneider cells. Immunocytochemistry was performed on Schneider cells that were transiently transfected with pMK/Lon-Myc/Hy using anti-c-Myc monoclonal antibody (Sigma), and counterstained with Mitotracker Red.

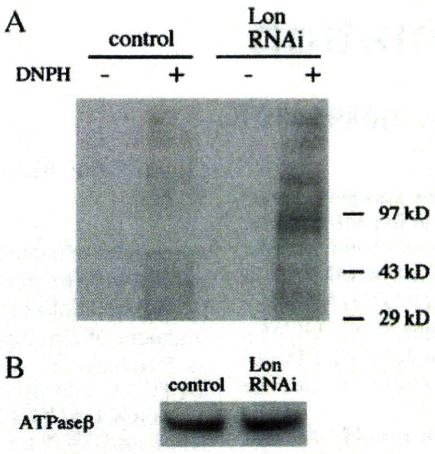

Fig. S2. Protein oxidation status in mitochondria from Lon knockdown cells. Mitochondrial fractions were prepared from Schneider cells carrying no vector (control) or pMt/invLon/Hy (Lon RNAi). (*A*) Detection of oxidized protein was performed using the Oxyblot protocol (Millipore). Mitochondrial protein extracts (10 μg) were incubated in the presence or absence of 2,4-dinitrophenylhydrazine (DNPH) to derivatize protein carbonyl groups. After fractionation by 4%–10% gradient SDS-PAGE, the proteins were transferred to a nitrocellulose filter, and oxidized proteins were detected with antibody against DNP. (*B*) Mitochondrial protein extracts (10 μg) were fractionated by 12% SDS-PAGE, transferred a nitrocellulose filter and probed with affinity-purified rabbit antiserum against ATPase β as a control.

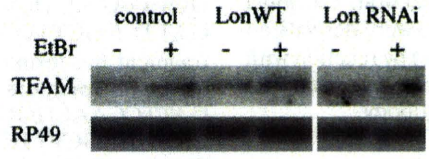

Fig. S3. Unchanged TFAM mRNA levels in Schneider cells upon EtBr treatment. After 6 d culture, Total RNA was isolated from Schneider cells with no plasmid (control) or carrying pMt/Lon/Hy (Lon) or pMt/invLon/Hy (Lon RNAi) that were cultured for 6 d in the presence or absence of 200 ng/mL EtBr. Northern blot analysis using *TFAM* and *RP49* probes was carried out as described in the legend to Fig. 1*D*.

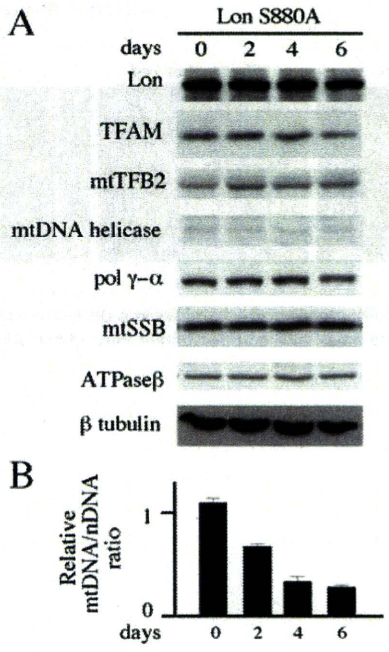

Fig. S4. Steady-state levels of mitochondrial nucleoid proteins during mtDNA depletion in Lon S880A- overexpressing Schneider cells. Schneider cells carrying pMt/S880A/Hy (S880A) were cultured for 6 d in the presence of 200 ng/mL EtBr. The cells were harvested prior to and after EtBr treatment at 0, 2, 4, and 6 days. (*A*) Immunoblot analysis was carried out as described in the legend to Fig. 1*A*. (*B*) Relative mtDNA copy number was determined as described in the legend to Fig. 1*C*.

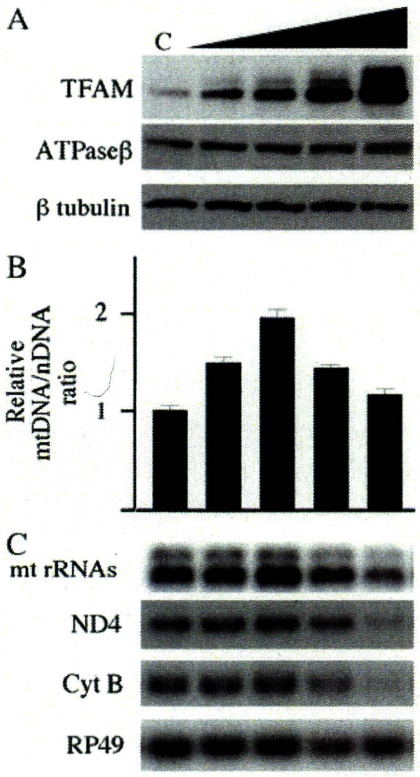

Fig. S5. Expression of *Drosophila* TFAM in Schneider cells. Schneider cells (*C*) or cells carring pMt/TFAM/Hy were grown for 10 d in the presence of 0, 0.05, 0.1, or 0.4 mM CuSO4. (*A*) Immunoblot analysis was carried out as described in the legend to Fig. 1*A*. (*B*) Relative mtDNA copy number was determined as described in the legend to Fig. 1*C*. Error bars indicate means ± standard error of two independent experiments. (*C*) Northern blot analysis using *12S rRNA, ND4, Cytb*, and *RP49* was carried out as described in the legend to Fig. 1*D*.

Vol 464|29 April 2010|doi:10.1038/nature08991

nature

ARTICLES

Adiponectin and AdipoR1 regulate PGC-1α and mitochondria by Ca^{2+} and AMPK/SIRT1

Masato Iwabu[1,2]*, Toshimasa Yamauchi[1,2]*, Miki Okada-Iwabu[1,2]*, Koji Sato[6], Tatsuro Nakagawa[7], Masaaki Funata[1], Mamiko Yamaguchi[1], Shigeyuki Namiki[3], Ryo Nakayama[1], Mitsuhisa Tabata[8], Hitomi Ogata[9], Naoto Kubota[1], Iseki Takamoto[1], Yukiko K. Hayashi[10], Naoko Yamauchi[4], Hironori Waki[1], Masashi Fukayama[4], Ichizo Nishino[10], Kumpei Tokuyama[9], Kohjiro Ueki[1], Yuichi Oike[8], Satoshi Ishii[5], Kenzo Hirose[3], Takao Shimizu[5], Kazushige Touhara[6,7] & Takashi Kadowaki[1]

Adiponectin is an anti-diabetic adipokine. Its receptors possess a seven-transmembrane topology with the amino terminus located intracellularly, which is the opposite of G-protein-coupled receptors. Here we provide evidence that adiponectin induces extracellular Ca^{2+} influx by adiponectin receptor 1 (AdipoR1), which was necessary for subsequent activation of Ca^{2+}/calmodulin-dependent protein kinase kinase β (CaMKKβ), AMPK and SIRT1, increased expression and decreased acetylation of peroxisome proliferator-activated receptor γ coactivator-1α (PGC-1α), and increased mitochondria in myocytes. Moreover, muscle-specific disruption of AdipoR1 suppressed the adiponectin-mediated increase in intracellular Ca^{2+} concentration, and decreased the activation of CaMKK, AMPK and SIRT1 by adiponectin. Suppression of AdipoR1 also resulted in decreased PGC-1α expression and deacetylation, decreased mitochondrial content and enzymes, decreased oxidative type I myofibres, and decreased oxidative stress-detoxifying enzymes in skeletal muscle, which were associated with insulin resistance and decreased exercise endurance. Decreased levels of adiponectin and AdipoR1 in obesity may have causal roles in mitochondrial dysfunction and insulin resistance seen in diabetes.

Adiponectin (encoded by *Adipoq*)[1–4] is an anti-diabetic and anti-atherogenic adipokine. Plasma adiponectin levels are decreased in obesity, insulin resistance, and type 2 diabetes[5]. Administration of adiponectin has been shown to cause glucose-lowering effects and ameliorate insulin resistance in mice[6–8]. Conversely, adiponectin-deficient mice exhibit insulin resistance and diabetes[9,10]. This insulin-sensitizing effect of adiponectin seems to be mediated by an increase in fatty acid oxidation by activation of AMP-activated protein kinase (AMPK)[11–13] and also by peroxisome proliferator-activated receptor α (PPARα)[14,15].

We previously reported the cloning of complementary DNAs encoding adiponectin receptors 1 and 2 (*Adipor1* and *Adipor2*) by expression cloning[16]. AdipoR1 is abundantly expressed in skeletal muscle and liver, whereas AdipoR2 is predominantly expressed in the liver. Both receptors are predicted to contain seven-transmembrane domains[16], but to be structurally and functionally distinct from G-protein-coupled receptors[17–19]. Adiponectin receptors may thus be thought to comprise a new receptor family.

We previously showed using *Adipor1* and/or *Adipor2* knockout mice that AdipoR1 and AdipoR2 act as the major receptors for adiponectin *in vivo*, and have important roles in the regulation of glucose and lipid metabolism, inflammation and oxidative stress *in vivo*[20]. Moreover, in the liver, AdipoR1 activated AMPK pathways and AdipoR2 activated PPARα pathways[20]. Therefore, identification of the 'missing link' between adiponectin receptors and adiponectin-activated key molecules is an important next step towards our understanding of the actions of adiponectin.

Insulin resistance has been reported to be associated with mitochondrial dysfunction[21]. However, the exact cause of mitochondrial dysfunction has yet to be ascertained. To clarify whether decreased adiponectin/AdipoR1 signalling could be associated with mitochondrial dysfunction, we analysed muscle-specific *Adipor1*-knockout (muscle-R1KO) mice, and attempted to determine the signalling mechanisms by which adiponectin/AdipoR1 would exert their biological effects.

Decreased PGC-1α and mitochondria in muscle-R1KO

Muscle-R1KO mice showed decreased phosphorylation of AMPK (Fig. 1a). Moreover, the administration of adiponectin increased the phosphorylation of AMPK in the muscle of control littermates but not in those of muscle-R1KO mice (Supplementary Fig. 1a), whereas adiponectin increased the phosphorylation of AMPK in the liver of both genotypes (Supplementary Fig. 1b). Muscle-R1KO mice also exhibited decreased molecules involved in mitochondrial biogenesis, such as PGC-1α[22], at both messenger RNA (*Ppargc1a*) (Fig. 1b) and protein levels (Fig. 1c). Adiponectin increased the expression levels of *Ppargc1a* in muscles of control littermates but not in those of muscle-R1KO mice (Supplementary Fig. 1c).

Muscle-R1KO mice showed decreases in molecules involved in mitochondrial biogenesis such as oestrogen-related receptor α (*Esrra*)[23], molecules involved in transcription such as nuclear respiratory factor 1 (*Nrf1*), and molecules involved in mitochondrial DNA replication/translation such as mitochondrial transcription factor A (*Tfam*)

[1]Department of Diabetes and Metabolic Diseases, Graduate School of Medicine, [2]Department of Integrated Molecular Science on Metabolic Diseases, 22nd Century Medical and Research Center, [3]Department of Neurobiology, Graduate School of Medicine, [4]Department of Pathology, Graduate School of Medicine, [5]Department of Biochemistry and Molecular Biology, Faculty of Medicine, The University of Tokyo, Tokyo 113-0033, Japan. [6]Department of Applied Biological Chemistry, Graduate School of Agricultural and Life Sciences, The University of Tokyo, Tokyo 113-8657, Japan. [7]Department of Integrated Biosciences, The University of Tokyo, Chiba 277-8562, Japan. [8]Department of Molecular Genetics, Graduate School of Medical Sciences, Kumamoto University, Kumamoto 860-0811, Japan. [9]Graduate School of Comprehensive Human Sciences, University of Tsukuba, Tsukuba 305-8577, Japan. [10]Department of Neuromuscular Research, National Institute of Neuroscience, National Center of Neurology and Psychiatry, Kodaira, Tokyo 187-8502, Japan.
*These authors contributed equally to this work.

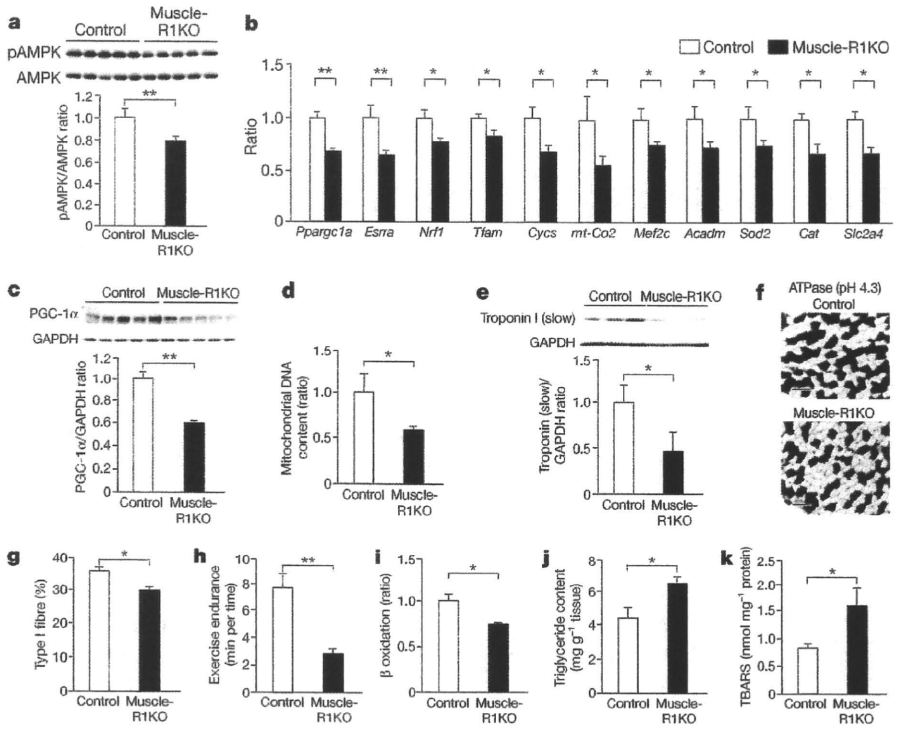

Figure 1 | Decreased mitochondria, oxidative type I myofibres and exercise capacity in skeletal muscle of muscle-R1KO mice. **a–k**, Phosphorylation and amount of AMPK (**a**), *Ppargc1a*, *Esrra*, *Nrf1*, *Tfam*, *Cycs*, *mt-Co2*, *Mef2c*, *Acadm*, *Sod2*, *Cat* and *Slc2a4* mRNA levels (**b**), PGC-1α protein levels (**c**), mitochondrial content as assessed by mitochondrial DNA copy number (**d**), amounts of troponin I (slow) protein (**e**), ATPase (pH 4.3 for type I fibres) staining of soleus muscles (scale bars, 100 μm) (**f**), quantification of type I fibres (**g**) based on fibre-type analyses (**f**), exercise endurance (**h**), β oxidation (**i**), triglyceride content (**j**), and TBARS (**k**) in skeletal muscle (**a–g**, **i–k**) obtained from control or muscle-R1KO after 5 h fasting. All values are presented as mean ± s.e.m. $n = 5$–12, $^{*}P < 0.05$ and $^{**}P < 0.01$ compared to control mice.

(Fig. 1b). Moreover, the expression levels of several oxidative phosphorylation and other mitochondrial genes were significantly reduced in muscle-R1KO mice, including cytochrome *c* (*Cycs*), and cytochrome *c* oxidase subunit II (*mt-Co2*) (Fig. 1b). Furthermore, muscle-R1KO mice had a decreased mitochondrial DNA content (Fig. 1d).

Mitochondrial function was assessed by measuring the enzymatic activities of Cox (Supplementary Fig. 2a) and succinate dehydrogenase (SDH) (Supplementary Fig. 2b). Staining of soleus muscle sections revealed a lower number of Cox- and SDH-positive muscle fibres and a decreased intensity of Cox and SDH staining in muscle-R1KO mice (Supplementary Fig. 2a, b).

Decreased type I fibres and exercise capacity in muscle-R1KO

Muscle-R1KO mice had decreased molecules involved in type I fibre[24] differentiation myocyte enhancer factor 2C (*Mef2c*)[25] (Fig. 1b) as well as the type I fibre marker troponin I (slow) (Fig. 1e). In contrast, muscle-R1KO mice had almost the same expression levels of MHCIIa, MHCIIx and MHCIIb as those seen in control mice (Supplementary Fig. 2c–e), indicating a reduction in oxidative, high endurance fibres in muscle-R1KO mice. These findings were consistent with the histological analysis performed (Fig. 1f, g). In soleus muscle of muscle-R1KO mice, type I fibres were reduced by 20% (Fig. 1g).

To study the effect of *Adipor1* ablation on skeletal muscle function in intact animals, we challenged control and muscle-R1KO mice with involuntary physical-exercise-assessed muscle endurance by treadmill running. Muscle endurance was significantly lower for muscle-R1KO mice than control mice (Fig. 1h).

We next examined the expression of metabolic genes and found that molecules involved in fatty-acid oxidation, such as medium-chain acyl-CoA dehydrogenase (*Acadm*), were significantly decreased in muscle-R1KO mice (Fig. 1b), which was associated with decreased β oxidation (Fig. 1i) and increased triglyceride content (Fig. 1j) in skeletal muscle.

Muscle-R1KO mice exhibited decreased expression levels of mitochondrial and cytoplasmic oxidative-stress-detoxifying genes such as manganese superoxide dismutase (*Sod2*) (Fig. 1b) and catalase (*Cat*) (Fig. 1b), respectively, and increased oxidative stress such as thiobarbituric acid reactive substance (TBARS) (Fig. 1k) in muscle. Expression of the insulin-sensitive glucose transporter 4 (*Slc2a4*) was reduced in muscle-R1KO mice (Fig. 1b).

Insulin resistance in muscle-R1KO mice

Plasma glucose and insulin levels after glucose administration were significantly higher in muscle-R1KO mice than in control mice (Fig. 2a, b). The capacities of muscle-R1KO mice to regulate plasma glucose levels after a bolus of insulin were significantly decreased as compared with control mice (Fig. 2c).

We performed a hyperinsulinaemic-euglycaemic clamp experiment. Disruption of *Adipor1* in muscle did not significantly alter endogenous glucose production, whereas it significantly decreased the glucose disposal rate and the glucose infusion rate, indicating decreased insulin sensitivity in muscle (Fig. 2d–f).

In agreement with the data obtained from the hyperinsulinaemic-euglycaemic clamps, decreased tyrosine phosphorylation of IRS-1 (Fig. 2g) and decreased phosphorylation of Ser 473 in Akt (Fig. 2h) stimulated with insulin in skeletal muscle of muscle-R1KO mice were found, which seemed to be associated with increased phosphorylation of S6K1 (Fig. 2i) and JNK (Fig. 2j). Ser 302 in mice IRS-1 has been reported to be phosphorylated by JNK[26], and the phosphorylation of Ser 636/639 has been reported to be mediated by mTOR and S6K1 pathways[27], both of which would result in inhibition of insulin signalling. The amounts of Ser 302 and Ser 636/639 phosphorylation in IRS-1 were increased in skeletal muscle of muscle-R1KO mice (Fig. 2k, l).

CaMKKβ is required for adiponectin/AdipoR1-induced PGC-1α

We next investigated the molecular mechanisms by which muscle-R1KO mice exhibited these phenotypes described earlier. Incubation of C2C12 myocytes with 30 μg ml^{-1} adiponectin increased mitochondrial DNA content (Fig. 3a). AMPK activity is dependent on the phosphorylation of AMPKα(Thr 172) in its activation loop by AMPK kinases (AMPKKs)[13,28]. LKB1 and CaMKKβ are known to be two major AMPKKs present in a variety of tissues and cells[13,29,30]. Suppression of AdipoR1 or CaMKKβ, or both AMPKα1 and AMPKα2 or PGC-1α expression by each specific short interfering RNA (siRNA) (Supplementary Fig. 3a–e) markedly reduced the increases in mitochondrial DNA content induced by adiponectin (Fig. 3a). In contrast, the suppression of AdipoR2 expression by

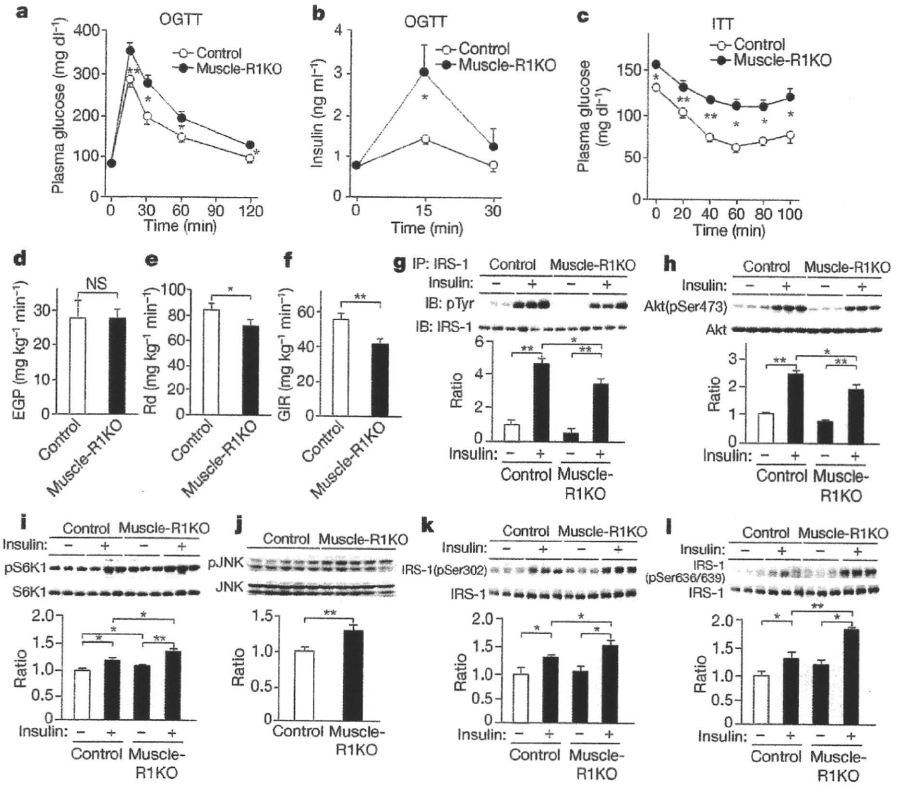

Figure 2 | Mechanisms of abnormal glucose and insulin homeostasis in muscle-R1KO mice. **a–f**, Plasma glucose (**a**, **c**) and plasma insulin (**b**) during an oral glucose tolerance test (OGTT) (1.5 g glucose per kg body weight) (**a**, **b**) or during an insulin tolerance test (ITT) (0.25 U insulin per kg body weight) (**c**), endogenous glucose production (EGP) (**d**), rates of glucose disposal (Rd) (**e**) and glucose infusion rate (GIR) (**f**) during a hyperinsulinaemic-euglycaemic clamp study in control and muscle-R1KO mice. **g–l**, Phosphorylation of tyrosine (pTyr) (**g**), Ser 302 (**k**) and Ser 636/639 (**l**) in IRS-1, phosphorylation and amount of Akt (**h**), S6K1 (**i**) and JNK (**j**) in skeletal muscle treated with or without insulin (0.3 U per kg body weight) for 7.5 min in control and muscle-R1KO mice after 5 h fasting. IB, immunoblot; IP, immunoprecipitate. All values are presented as mean ± s.e.m. $n = 6$–15 from 3–5 independent experiments, $^*P < 0.05$ and $^{**}P < 0.01$ compared to control or as indicated. NS, not significant.

specific siRNA (Supplementary Fig. 3f) failed to significantly reduce mitochondrial biogenesis induced by adiponectin (Fig. 3a).

Suppression of AdipoR1 or CaMKKβ expression by each specific siRNA (Supplementary Fig. 3a, b) greatly reduced the increase in PGC-1α expression induced by adiponectin (Fig. 3b). Interestingly, the suppression of AMPKα1 and AMPKα2 expression by each specific siRNA (Supplementary Fig. 3c, d) failed to significantly reduce PGC-1α expression induced by adiponectin (Fig. 3b), suggesting that PGC-1α expression was induced by adiponectin via an AdipoR1- and CaMKKβ-dependent yet AMPK-independent pathway.

PGC-1α has been reported to be activated by AMPK via phosphorylation[31] and by deacetylation through SIRT1 activation[32]. We next addressed the possibility that AMPK activated by adiponectin and AdipoR1 could regulate PGC-1α activities. Treatment of C2C12 myocytes with adiponectin decreased PGC-1α acetylation after 2 h of treatment (Fig. 3c). Suppression of AdipoR1 or both AMPKα1 and AMPKα2 or SIRT1 expression by each specific siRNA (Supplementary Fig. 3a, c, d, g) largely abrogated the decrease in PGC-1α acetylation induced by adiponectin (Fig. 3c). The PGC-1α-2A mutant lacking the two AMPK phosphorylation sites[31] showed markedly reduced PGC-1α deacetylation and mitochondrial biogenesis with adiponectin (Fig. 3d, e).

Adiponectin failed to induce mitochondrial biogenesis further in the C2C12 myocytes expressing PGC-1α-R13 in which 13 of the potential lysine acetylation sites were mutated into arginine[32] (Fig. 3f). Because the capacity for undergoing acetylation is impaired in the PGC-1α-R13 mutant, these data are consistent with the dependence of adiponectin on SIRT1-mediated deacetylation of PGC-1α in activating PGC-1α.

SIRT1 deacetylase activity has been reported to be driven by NAD^+ levels[32,33]. Adiponectin increased the NAD^+/NADH ratio in C2C12 myocytes (Fig. 3g). Muscle-R1KO mice also showed increased PGC-1α acetylation (Fig. 3h) and decreased the NAD^+/NADH ratio stimulated with adiponectin (Fig. 3i) *in vivo*. These data indicated that the total activity as assessed by multiplying expression and deacetylation of PGC-1α is markedly reduced in muscle-R1KO mice (Supplementary Fig. 4).

Adiponectin induces Ca^{2+} influx by AdipoR1

Interestingly, treatment of C2C12 myocytes with adiponectin resulted in an increase in the intracellular Ca^{2+} concentration measured by fura-2-based fluorescent imaging (Fig. 4a). C2C12 myocytes showed responses to adiponectin in a dose-dependent manner (data not shown). Removal of extracellular free Ca^{2+} by EGTA almost completely abolished the adiponectin-induced Ca^{2+} response (Fig. 4a), whereas EGTA had no effect on the ATP-induced intracellular Ca^{2+} release (data not shown). Suppression of AdipoR1 expression using a specific siRNA (Fig. 4b) largely reduced the calcium response of C2C12 myocytes to adiponectin (Fig. 4c, d). These results indicate that the influx of extracellular Ca^{2+} after adiponectin treatment of C2C12 myocytes is mediated by AdipoR1.

To study further the importance of AdipoR1 for adiponectin-induced Ca^{2+} response in the gain-of-function experiments, we expressed AdipoR1 in *Xenopus laevis* oocytes (Fig. 4e). The increase in intracellular calcium levels stimulated with adiponectin was detected by monitoring Ca^{2+}-activated Cl^- currents in AdipoR1 complementary-RNA-injected oocytes (Fig. 4f, g). The responses were not observed in control oocytes (Fig. 4g). We studied the effect of removal of extracellular free Ca^{2+} by EGTA on the Ca^{2+}-activated Cl^- current response to adiponectin of *Xenopus* oocytes expressing AdipoR1. We found that the removal of extracellular free Ca^{2+} by EGTA almost completely abolished the Ca^{2+}-activated Cl^- current response to adiponectin of *Xenopus* oocytes expressing AdipoR1 (Fig. 4g), indicating that these responses were dependent on extracellular Ca^{2+}.

Adiponectin-induced Ca^{2+} influx is important for its actions

Incubation of C2C12 myocytes with adiponectin increased the phosphorylation of the AMPK α-subunit at Thr 172, and EGTA partially suppressed adiponectin-induced increased AMPK phosphorylation (Fig. 5a). As expected, EGTA almost completely abolished ionomycin-dependent phosphorylation of AMPK, whereas EGTA had no effect on 5-aminoimidazole-4-carboxamide-1-β-D-riboside (AICAR)-induced phosphorylation of AMPK in C2C12 myocytes (Fig. 5a).

Suppression of CaMKKβ or LKB1 expression by each specific siRNA (Supplementary Fig. 3b, h) significantly reduced the increases in

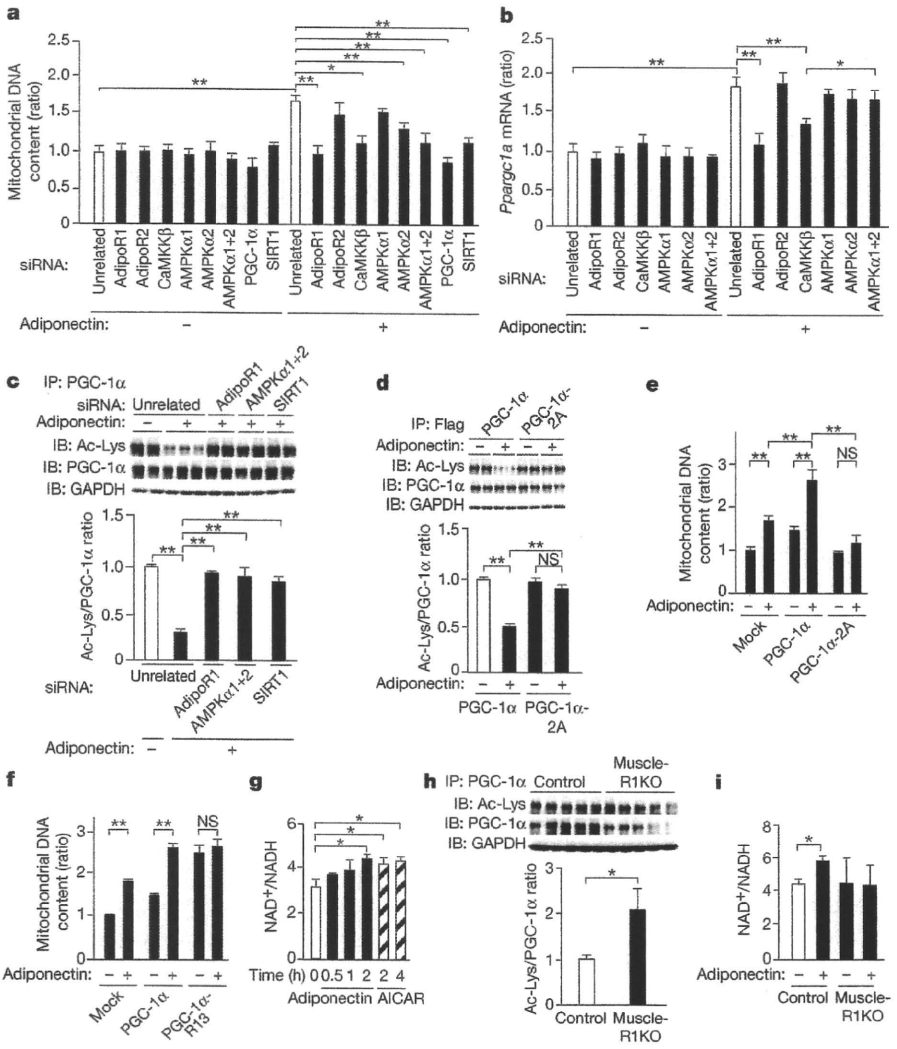

Figure 3 | Adiponectin/AdipoR1 increase PGC-1α expression and activity, and mitochondrial biogenesis in C2C12 myocytes.
a–i, Mitochondrial content as assessed by mitochondrial DNA copy number (**a**, **e**, **f**), *Ppargc1a* mRNA levels (**b**), acetyl-lysine (Ac-Lys) levels checked on PGC-1α or Flag immunoprecipitates (**c**, **d**, **h**), NAD^+/NADH ratio (**g**, **i**) in C2C12 myocytes treated with adiponectin for the times indicated (**g**), in C2C12 myocytes transfected with the indicated siRNA duplex (**a–c**), in C2C12 myocytes transfected with the wild-type or the 2A mutant form of PGC-1α (**d**, **e**) or the R13 mutant form of PGC-1α (**f**) treated with 10 μg ml^{-1} adiponectin for 48 h (**a**, **e**, **f**) or for 1.5 h (**b**) or 2 h (**c**, **d**), or in skeletal muscle from control or muscle-R1KO mice treated with or without adiponectin (**h**, **i**). The supernatant was blotted against GAPDH as an input control (**c**, **d**, **h**). C2C12 myocytes were used after myogenic differentiation in all experiments. All values are presented as mean ± s.e.m. $n = 5–10$, $^*P < 0.05$ and $^{**}P < 0.01$ compared to control or unrelated siRNA or as indicated.

phosphorylation of AMPK induced by adiponectin (Fig. 5b). Although the AMPK inhibitor AraA only tended to reduce adiponectin-induced PGC-1α expression, Ca^{2+} removal by EGTA or inhibition of CaMKKβ with its selective inhibitor STO-609 (ref. 34) effectively and almost completely abolished increased PGC-1α expression stimulated with adiponectin in C2C12 myocytes (Fig. 5c), as removal of extracellular Ca^{2+} effectively abolishes the Ca^{2+} signal evoked by adiponectin (Fig. 4a).

Finally, we examined whether adiponectin-induced Ca^{2+} influxes into skeletal muscle might be impaired in muscle-R1KO mice through *in vivo* imaging[35,36]. We found that whereas treatment of soleus muscle with adiponectin resulted in an increase in the intracellular Ca^{2+} concentration as measured by fura-2-based fluorescent imaging in control mice, muscle-R1KO mice almost completely abrogated the calcium response of soleus muscle to adiponectin (Fig. 5d–f), consistent with the observation that adiponectin significantly increased the phosphorylation of CaMKI[37,38], an intracellular substrate of CaMKKβ, by AdipoR1 in skeletal muscle *in vivo* (Supplementary Fig. 5).

We also attempted to examine whether simultaneous activation of Ca^{2+} signalling and AMPK/SIRT1 pathways by exercise, independent of AdipoR1, could rescue phenotype in muscle-R1KO mice. Two weeks of exercise significantly ameliorated insulin resistance, and increased mitochondrial content and function such as citrate synthase activities in muscles of muscle-R1KO mice (Fig. 6a–d).

Discussion

Here we provide evidence that muscle-R1KO mice exhibit decreased mitochondrial content and enzymes. PGC-1α is a key regulator of mitochondrial content and function. Expression of PGC-1α has been reported to be modulated in several physiological contexts, for example, in skeletal muscle in response to exercise partly by increased Ca^{2+} signalling via molecules such as CaMK and CREB[39]. Activities of PGC-1α have also been reported to be modulated by several kinds of PGC-1α modifications, such as phosphorylation by AMPK[31] and deacetylation by AMPK and SIRT1[32]. AMPK and SIRT1 could also be activated by exercise. We have demonstrated that muscle-R1KO mice exhibit decreased PGC-1α expression as well as decreased deacetylation of PGC-1α. Consistent with this, adiponectin induced Ca^{2+} influx by AdipoR1, thereby activating CaMKKβ, which led to increased PGC-1α expression. Moreover, adiponectin/AdipoR1 activated AMPK and SIRT1, thereby inducing PGC-1α deacetylation. These data indicated that adiponectin and AdipoR1 stimulate increases in both the expression and activation of PGC-1α, in a similar fashion to exercise (Fig. 6e).

Although the degree of decreased PGC-1α expression was approximately 40% in muscle-R1KO mice, the extent of decreased mitochondrial biogenesis and decreased exercise endurance were comparable to those observed in muscle-specific PGC-1α-knockout mice[40], which may be explained by the finding that adiponectin and AdipoR1 increase not only PGC-1α expression but also PGC-1α activity (Fig. 6e).

Importantly, decreases in the expression of AdipoR1 and PGC-1α and mitochondrial DNA content were also observed in type 2 diabetic patients[41] and individuals at increased risk of developing diabetes owing to their family history[42], as well as in obese diabetic *db/db* mice (Supplementary Fig. 6a–c). These data indicate that decreased

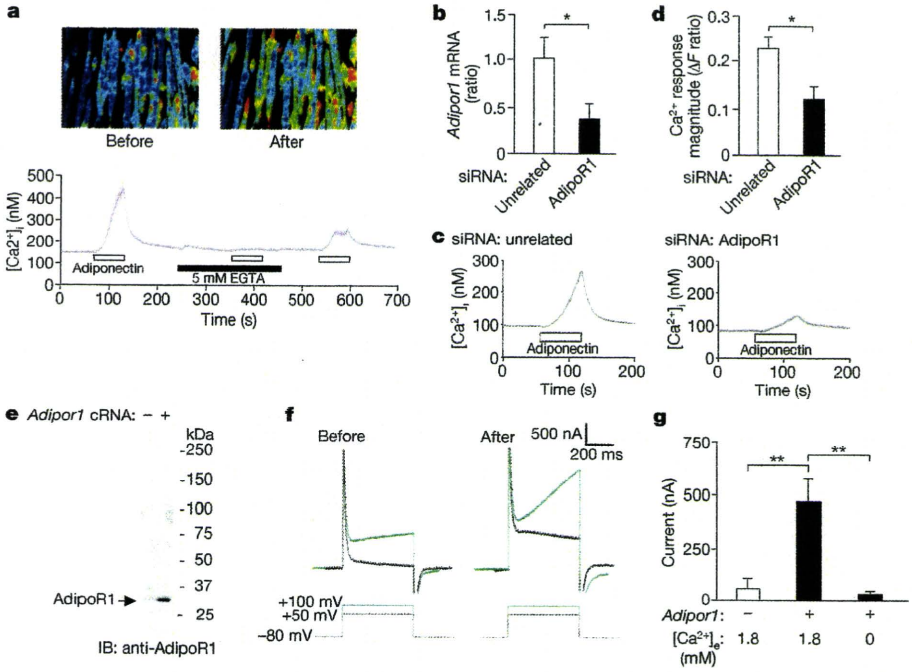

Figure 4 | Adiponectin-induced Ca^{2+} influx by AdipoR1 in C2C12 myocytes and *Xenopus* oocytes. **a**, Pseudocoloured images of changes in fura-2 before and after 1 min stimulation with adiponectin (30 μg ml^{-1}). Red corresponds to the greatest response. The bottom trace demonstrates the average calcium response of C2C12 myocytes to 1-min stimulation with adiponectin along with application of 5 mM EGTA (black bar). The shaded region around the trace represents s.e.m. **b–d**, *Adipor1* mRNA levels (**b**), fura-2 calcium response (**c**) and their magnitude (**d**) of C2C12 myocytes transfected with unrelated siRNA duplex or AdipoR1 siRNA duplex to stimulation with 30 μg ml^{-1} adiponectin for 1 min. **e–g**, The amounts of AdipoR1 protein (**e**), representative Ca^{2+}-activated Cl^- current traces (**f**) before (left) and after (right) 30-s application of adiponectin, and their magnitude (**g**) in *Xenopus* oocytes injected with or without *Adipor1* cRNA in response to adiponectin (30 μg ml^{-1}), and with or without application of 5 mM EGTA with depolarizing pulses of +100 mV. $[Ca^{2+}]_i$ and $[Ca^{2+}]_e$, intracellular and external Ca^{2+} concentration, respectively. All values are presented as mean ± s.e.m. $n = 6–14$, $^*P < 0.05$ and $^{**}P < 0.01$ compared to unrelated siRNA cells or control cells or as indicated.

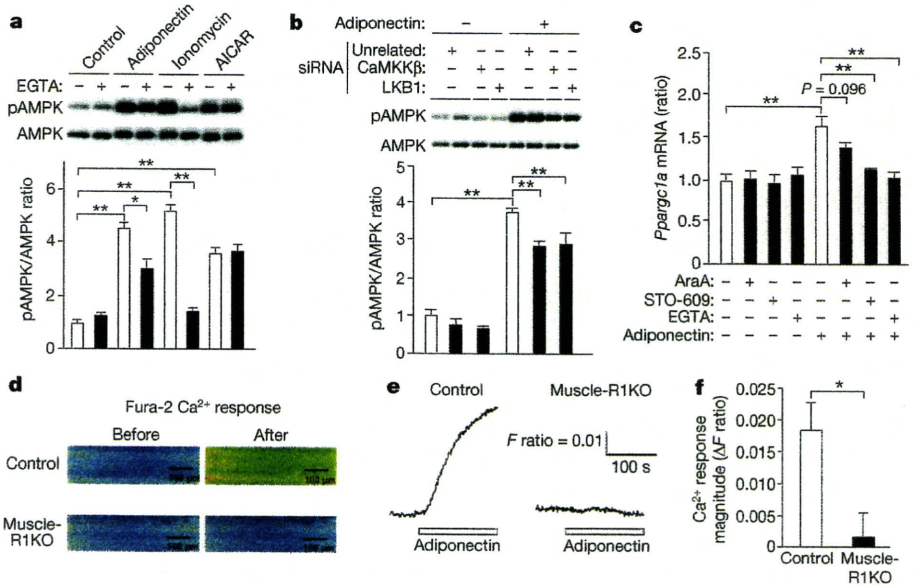

Figure 5 | Adiponectin-induced Ca^{2+} influx is required for CaMKK and AMPK activation and PGC-1α expression. **a**, **b**, Phosphorylation and amount of AMPK in C2C12 myocytes preincubated for 20 min with or without 5 mM EGTA and then treated for 5 min with adiponectin (30 μg ml^{-1}) or ionomycin (1 μM), or for 1 h with AICAR (1 mM) (**a**), or C2C12 myocytes transfected with the indicated siRNA duplex and then treated with 30 μg ml^{-1} adiponectin for 5 min (**b**). **c**, Amount of *Ppargc1a* mRNA in C2C12 myocytes preincubated for 1 h with AraA (0.5 mM) or for 6 h with STO-609 (1 μg ml^{-1}) or for 20 min with EGTA (5 mM), and then treated for 1.5 h with or without adiponectin (10 μg ml^{-1}). **d**, Representative pseudocoloured images of changes in the fura-2 calcium response before and after 5 min stimulation with adiponectin (30 μg ml^{-1}) in a soleus muscle from control mice (top) and muscle-R1KO mice (bottom). Red corresponds to the greatest response. Scale bars, 100 μm. **e**, Trace demonstrates the calcium response of soleus muscle in the fields presented in **d**. Adiponectin was applied during the indicated period. **f**, The magnitude of fura-2 calcium response signals by 160-s adiponectin stimulation to soleus muscles. ΔF ratio indicates the change in the fluorescence ratio after adiponectin application. All values are presented as mean ± s.e.m. $n = 5–10$, $^*P < 0.05$ and $^{**}P < 0.01$ compared to control or unrelated siRNA cells or as indicated.

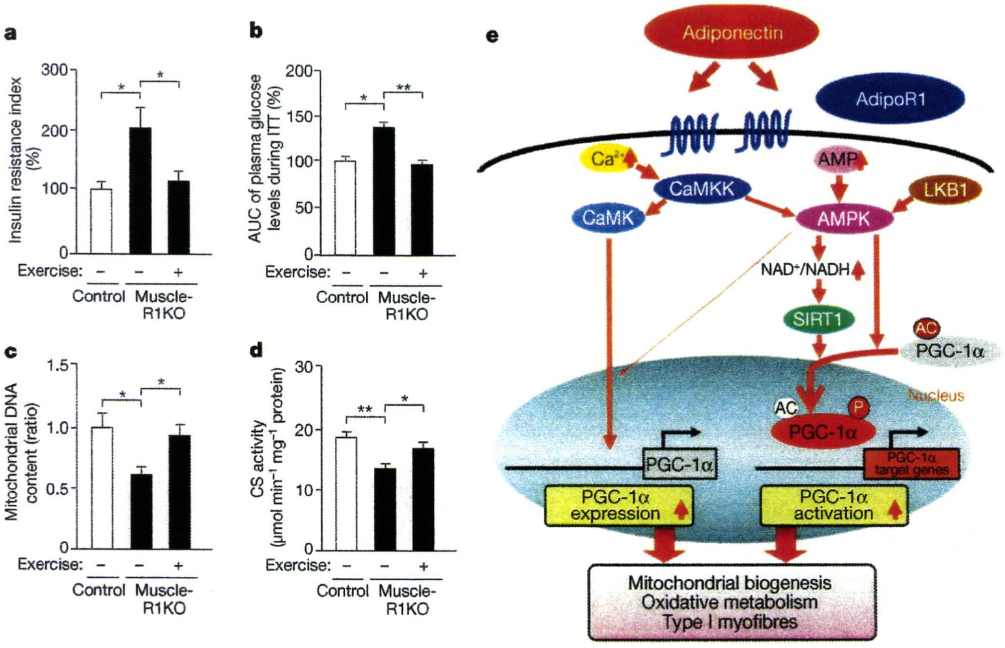

Figure 6 | The effect of exercise on muscle-R1KO mice. a–d, The insulin resistance index (**a**), area under the curves (AUC) of plasma glucose levels during the ITT (**b**), mitochondrial content as assessed by mitochondrial DNA copy number (**c**), and citrate synthase (CS) enzyme activity (**d**) in skeletal muscle of control and muscle-R1KO mice after 2 weeks exercise. The results are expressed as the percentage of the value in control littermates (**a, b**). **e,** Scheme illustrating the signal transduction of adiponectin/AdipoR1 in muscle cells. Both CaMKKβ and LKB1 are necessary for adiponectin-induced full AMPK activation. AMPK and SIRT1 are required for adiponectin/AdipoR1-induced PGC-1α activation. CaMKKβ activation by adiponectin-induced Ca^{2+} influx via AdipoR1 is required for adiponectin-induced increased PGC-1α expression. PGC-1α is required for mitochondrial biogenesis stimulated with adiponectin/AdipoR1. From these data, we conclude that adiponectin and AdipoR1 increase PGC-1α expression and activity by Ca^{2+} signalling and by AMPK and SIRT1, leading to increased mitochondrial biogenesis. We focused on the molecules that we have obtained direct evidence by both gain-of-function and loss-of-function experiments *in vitro* and *in vivo*, except for CaMK, which has already been reported to increase PGC-1α expression by other researchers[39]. AC, acetylation. All values are presented as mean ± s.e.m. $n = 5–8$, $^*P < 0.05$ and $^{**}P < 0.01$ compared to control mice or as indicated.

adiponectin/AdipoR1 in pathophysiological conditions such as obesity may have causal roles in the development of PGC-1α dysregulation and mitochondrial dysfunction.

In skeletal muscle AdipoR1 regulated insulin sensitivity by several mechanisms (Supplementary Fig. 7). First is the activation of S6K1, which has been reported to be able to cause insulin resistance by increased phosphorylation of Ser 636/639 in IRS-1 (ref. 27). S6K1 is crucially inhibited by AMPK[43]. In skeletal muscle of muscle-R1KO mice, AMPK activation was reduced, whereas activation of S6K1 and phosphorylation of Ser 636/639 in IRS-1 were indeed increased. Second is the increased oxidative stress, which has been causally linked to insulin resistance[44] by increased phosphorylation of Ser 302 in IRS-1 through JNK activation[26]. Several oxidative stress detoxification genes are crucially regulated by AMPK and PGC-1α[45], and the expression levels of these genes such as *Sod2* and *Cat* were reduced, which was associated with increased TBARS in skeletal muscle of muscle-R1KO mice. Third is the increased triglyceride content, which has been associated with insulin resistance by increased phosphorylation of Ser 302 in IRS-1 through JNK activation[26]. Molecules involved in fatty-acid oxidation are crucially regulated by AMPK and PGC-1α, and the expression levels of these genes such as *Mcad* were reduced, which was associated with increased triglyceride content in skeletal muscle of muscle-R1KO mice. Consistent with increased TBARS and triglyceride content, JNK activation and phosphorylation of Ser 302 in IRS-1 were indeed increased.

Exercise has been reported to have beneficial effects on longevity and lifestyle-related diseases, and at the same time to activate Ca^{2+}, AMPK, SIRT1 and PGC-1α pathways[39]. In this study, we clearly demonstrated that adiponectin and AdipoR1 regulate PGC-1α and mitochondria via Ca^{2+} and AMPK/SIRT1. Therefore, agonism of AdipoR1 as well as strategies to increase AdipoR1 in muscle could be exercise-mimetics.

In conclusion, AdipoR1 has a crucial role in the physiological and pathophysiological significance of adiponectin in muscle, and is involved in the regulation of Ca^{2+} signalling, PGC-1α expression and activation, mitochondrial function and oxidative stress, glucose and lipid metabolism, and exercise endurance. This study suggests that agonism of AdipoR1, as well as strategies to increase AdipoR1 in muscle, may be logical approaches to providing a new treatment modality for mitochondrial dysfunction, insulin resistance and type 2 diabetes linked to obesity.

METHODS SUMMARY

Mice. Mice were 8–10 weeks of age at the time of the experiment. The animal care and use procedures were approved by the Animal Care Committee of the University of Tokyo.

Measurement of exercise capacity in muscle-R1KO mice. The treadmill exercise test regimen was 15 m min^{-1} for 20 min. Exercise endurance was assessed by dividing 20 min by the number of times a mouse was unable to avoid electrical shocks.

Studies with C2C12 cells. Induction of myogenic differentiation was carried out according to a method described previously[11]. By day 5, the cells had differentiated into multinucleated contracting myocytes. C2C12 myocytes were used after myogenic differentiation in all experiments.

Plasmids. The plasmids encoding PGC-1α and the PGC-1α-2A mutant were generous gifts from B. M. Spiegelman, and have all been described previously[31]. The plasmids encoding for the PGC-1α-R13 mutant were generous gifts from P. Puigserver, and have all been described previously[32].

Statistical analysis. Results are expressed as mean ± s.e.m. Differences between two groups were assessed using unpaired two-tailed *t*-tests. Data involving more than two groups were assessed by analysis of variance (ANOVA).

Received 12 August 2009; accepted 11 March 2010.
Published online 31 March 2010.

1. Scherer, P. E., Williams, S., Fogliano, M., Baldini, G. & Lodish, H. F. A novel serum protein similar to C1q, produced exclusively in adipocytes. *J. Biol. Chem.* 270, 26746–26749 (1995).

2. Hu, E., Liang, P. & Spiegelman, B. M. AdipoQ is a novel adipose-specific gene dysregulated in obesity. *J. Biol. Chem.* **271,** 10697–10703 (1996).
3. Maeda, K. *et al.* cDNA cloning and expression of a novel adipose specific collagen-like factor, apM1 (AdiPose Most abundant Gene transcript 1). *Biochem. Biophys. Res. Commun.* **221,** 286–289 (1996).
4. Nakano, Y., Tobe, T., Choi-Miura, N.-H., Mazda, T. & Tomita, M. Isolation and characterization of GBP28, a novel gelatin-binding protein purified from human plasma. *J. Biochem.* **120,** 803–812 (1996).
5. Hotta, K. *et al.* Plasma concentrations of a novel, adipose-specific protein, adiponectin, in type 2 diabetic patients. *Arterioscler. Thromb. Vasc. Biol.* **20,** 1595–1599 (2000).
6. Fruebis, J. *et al.* Proteolytic cleavage product of 30-kDa adipocyte complement-related protein increases fatty acid oxidation in muscle and causes weight loss in mice. *Proc. Natl Acad. Sci. USA* **98,** 2005–2010 (2001).
7. Yamauchi, T. *et al.* The fat-derived hormone adiponectin reverses insulin resistance associated with both lipoatrophy and obesity. *Nature Med.* **7,** 941–946 (2001).
8. Berg, A. H., Combs, T. P., Du, X., Brownlee, M. & Scherer, P. E. The adipocyte-secreted protein Acrp30 enhances hepatic insulin action. *Nature Med.* **7,** 947–953 (2001).
9. Kubota, N. *et al.* Disruption of adiponectin causes insulin resistance and neointimal formation. *J. Biol. Chem.* **277,** 25863–25866 (2002).
10. Maeda, N. *et al.* Diet-induced insulin resistance in mice lacking adiponectin/ACRP30. *Nature Med.* **8,** 731–737 (2002).
11. Yamauchi, T. *et al.* Adiponectin stimulates glucose utilization and fatty-acid oxidation by activating AMP-activated protein kinase. *Nature Med.* **8,** 1288–1295 (2002).
12. Tomas, E. *et al.* Enhanced muscle fat oxidation and glucose transport by ACRP30 globular domain: acetyl-CoA carboxylase inhibition and AMP-activated protein kinase activation. *Proc. Natl Acad. Sci. USA* **99,** 16309–16313 (2002).
13. Kahn, B. B., Alquier, T., Carling, D. & Hardie, D. G. AMP-activated protein kinase: ancient energy gauge provides clues to modern understanding of metabolism. *Cell Metab.* **1,** 15–25 (2005).
14. Kersten, S., Desvergne, B. & Wahli, W. Roles of PPARs in health and disease. *Nature* **405,** 421–424 (2000).
15. Yamauchi, T. *et al.* Globular adiponectin protected ob/ob mice from diabetes and apoE deficient mice from atherosclerosis. *J. Biol. Chem.* **278,** 2461–2468 (2003).
16. Yamauchi, T. *et al.* Cloning of adiponectin receptors that mediate antidiabetic metabolic effects. *Nature* **423,** 762–769 (2003).
17. Wess, J. G-protein-coupled receptors: molecular mechanisms involved in receptor activation and selectivity of G-protein recognition. *FASEB J.* **11,** 346–354 (1997).
18. Yokomizo, T., Izumi, T., Chang, K., Takuwa, Y. & Shimizu, T. A. G-protein-coupled receptor for leukotriene B4 that mediates chemotaxis. *Nature* **387,** 620–624 (1997).
19. Scheer, A., Fanelli, F., Costa, T., De Benedetti, P. G. & Cotecchia, S. Constitutively active mutants of the α1B-adrenergic receptor: role of highly conserved polar amino acids in receptor activation. *EMBO J.* **15,** 3566–3578 (1996).
20. Yamauchi, T. *et al.* Targeted disruption of AdipoR1 and AdipoR2 causes abrogation of adiponectin binding and metabolic actions. *Nature Med.* **13,** 332–339 (2007).
21. Petersen, K. F. *et al.* Impaired mitochondrial activity in the insulin-resistant offspring of patients with type 2 diabetes. *N. Engl. J. Med.* **350,** 664–671 (2004).
22. Wu, Z. *et al.* Mechanisms controlling mitochondrial biogenesis and respiration through the thermogenic coactivator PGC-1. *Cell* **98,** 115–124 (1999).
23. Mootha, V. K. *et al.* Errα and Gabpa/b specify PGC-1α-dependent oxidative phosphorylation gene expression that is altered in diabetic muscle. *Proc. Natl Acad. Sci. USA* **101,** 6570–6575 (2004).
24. Berchtold, M. W. *et al.* Calcium ion in skeletal muscle: its crucial role for muscle function, plasticity, and disease. *Physiol. Rev.* **80,** 1215–1265 (2000).
25. Wu, H. *et al.* MEF2 responds to multiple calcium-regulated signals in the control of skeletal muscle fiber type. *EMBO J.* **19,** 1963–1973 (2000).
26. Hotamisligil, G. S. Inflammation and metabolic disorders. *Nature* **444,** 860–867 (2006).
27. Um, S. H. *et al.* Absence of S6K1 protects against age- and diet-induced obesity while enhancing insulin sensitivity. *Nature* **431,** 200–205 (2004).
28. Hawley, S. A. *et al.* Characterization of the AMP-activated protein kinase kinase from rat liver and identification of threonine 172 as the major site at which it phosphorylates AMP-activated protein kinase. *J. Biol. Chem.* **271,** 27879–27887 (1996).
29. Hawley, S. A. *et al.* Calmodulin-dependent protein kinase kinase-β is an alternative upstream kinase for AMP-activated protein kinase. *Cell Metab.* **2,** 9–19 (2005).
30. Woods, A. *et al.* Ca^{2+}/calmodulin-dependent protein kinase kinase-β acts upstream of AMP-activated protein kinase in mammalian cells. *Cell Metab.* **2,** 21–33 (2005).
31. Jäger, S., Handschin, C., St-Pierre, J. & Spiegelman, B. M. AMP-activated protein kinase (AMPK) action in skeletal muscle via direct phosphorylation of PGC-1α. *Proc. Natl Acad. Sci. USA* **104,** 12017–12022 (2007).
32. Rodgers, J. T. *et al.* Nutrient control of glucose homeostasis through a complex of PGC-1α and SIRT1. *Nature* **434,** 113–118 (2005).
33. Guarente, L. Sirtuins as potential targets for metabolic syndrome. *Nature* **444,** 868–874 (2006).
34. Tokumitsu, H. *et al.* STO-609, a specific inhibitor of the Ca^{2+}/calmodulin-dependent protein kinase kinase. *J. Biol. Chem.* **277,** 15813–15818 (2002).
35. Tóth, A. *et al.* Quantitative assessment of $[Ca^{2+}]_i$ levels in rat skeletal muscle *in vivo*. *Am. J. Physiol. Heart Circ. Physiol.* **275,** H1652–H1662 (1998).
36. Shkryl, V. M. & Shirokova, N. Transfer and tunneling of Ca^{2+} from sarcoplasmic reticulum to mitochondria in skeletal muscle. *J. Biol. Chem.* **281,** 1547–1554 (2006).
37. Anderson, K. A. *et al.* Components of a calmodulin-dependent protein kinase cascade. Molecular cloning, functional characterization and cellular localization of Ca^{2+}/calmodulin-dependent protein kinase kinase beta. *J. Biol. Chem.* **273,** 31880–31889 (1998).
38. Soderling, T. R. The Ca-calmodulin-dependent protein kinase cascade. *Trends Biochem. Sci.* **24,** 232–236 (1999).
39. Handschin, C. & Spiegelman, B. M. The role of exercise and PGC1α in inflammation and chronic disease. *Nature* **454,** 463–469 (2008).
40. Handschin, C. *et al.* Skeletal muscle fiber-type switching, exercise intolerance, and myopathy in PGC-1α muscle-specific knock-out animals. *J. Biol. Chem.* **282,** 30014–30021 (2007).
41. Mootha, V. K. *et al.* PGC-1α-responsive genes involved in oxidative phosphorylation are coordinately downregulated in human diabetes. *Nature Genet.* **34,** 267–273 (2003).
42. Patti, M. E. *et al.* Coordinated reduction of genes of oxidative metabolism in humans with insulin resistance and diabetes: Potential role of PGC1 and NRF1. *Proc. Natl Acad. Sci. USA* **100,** 8466–8471 (2003).
43. Wang, C. *et al.* Adiponectin sensitizes insulin signaling by reducing p70 S6 kinase-mediated serine phosphorylation of IRS-1. *J. Biol. Chem.* **282,** 7991–7996 (2007).
44. Houstis, N., Rosen, E. D. & Lander, E. S. Reactive oxygen species have a causal role in multiple forms of insulin resistance. *Nature* **440,** 944–948 (2006).
45. St-Pierre, J. *et al.* Suppression of reactive oxygen species and neurodegeneration by the PGC-1transcriptional coactivators. *Cell* **127,** 397–408 (2006).

Supplementary Information is linked to the online version of the paper at www.nature.com/nature.

Acknowledgements We thank B. M. Spiegelman for critical discussions and reading of the manuscript; T. Yokomizo for discussion and support; A. Tsuchida, K. Hara, Y. Hada, Y. Nio, T. Maki, T. Takazawa, Y. Iwata, M. Kobayashi, S. Kawamoto, K. Kobayashi, K. Hirota, Y. Shiomi, T. Mitsumatsu, L. Hirose, Y. Sea, M. Nakamura and K. Take for technical help and support; and S. Suzuki, K. Miyata, C. Ueda, A. Itoh and A. Okano for technical assistance. This work was supported by Grant-in-aid for Scientific Research (S) (20229008) (to T.K.), (B) (20390254) (to T.Y.), Targeted Proteins Research Program (to T.K.), the Global COE Research Program (to T.K.) and Translational Systems Biology and Medicine Initiative (to T.K.) from the Ministry of Education, Culture, Sports, Science and Technology of Japan.

Author Contributions M.I., M.O.-I., T.Y., K.S., T.N., M.F., M.Y., S.N., R.N., M.T., H.O., N.K., I.T., Y.K.H. and N.Y. performed experiments. T.K. and T.Y. conceived and supervised the study. K.T., T.S. and K.H. supervised the study. T.Y., T.K., M.I. and M.O-I. wrote the paper. All authors interpreted data.

Author Information Reprints and permissions information is available at www.nature.com/reprints. The authors declare no competing financial interests. Correspondence and requests for materials should be addressed to T.K. (kadowaki-3im@h.u-tokyo.ac.jp) or T.Y. (tyamau-tky@umin.net).

Acta Neuropathol (2010) 119:481–486
DOI 10.1007/s00401-010-0660-7

ORIGINAL PAPER

Congenital myotonic dystrophy can show congenital fiber type disproportion pathology

Kayo Tominaga · Yukiko K. Hayashi · Kanako Goto · Narihiro Minami · Satoru Noguchi · Ikuya Nonaka · Tetsuro Miki · Ichizo Nishino

Received: 19 November 2009 / Revised: 15 February 2010 / Accepted: 15 February 2010 / Published online: 24 February 2010

Abstract Congenital myotonic dystrophy (CDM) is associated with markedly expanded CTG repeats in *DMPK*. The presence of numerous immature fibers with peripheral halo is a characteristic feature of CDM muscles together with hypotrophy of type 1 fibers. Smaller type 1 fibers with no structural abnormality are a definitive criterion of congenital fiber type disproportion (CFTD). Nonetheless, we recently came across a patient who was genetically confirmed as CDM, but had been earlier diagnosed as CFTD when he was an infant. In this study, we performed clinical, pathological, and genetic analyses in infantile patients pathologically diagnosed as CFTD to evaluate CDM patients indistinguishable from CFTD. We examined CTG repeat expansion in *DMPK* in 28 infantile patients pathologically diagnosed as CFTD. Mutation screening of *ACTA1* and *TPM3* was performed, and we compared clinical and pathological findings of 20 CDM patients with those of the other cohorts. We identified four (14%) patients with CTG expansion in *DMPK*. *ACTA1* mutation was identified in four (14%), and *TPM3* mutation was found in two (7%) patients. Fiber size disproportion was more prominent in patients with *ACTA1* or *TPM3* mutations as compared to CFTD patients with CTG expansion. A further three patients among 20 CDM patients showed pathological findings similar to CFTD. From our results, CDM should be excluded in CFTD patients.

Keywords Congenital myotonic dystrophy (CDM) · Congenital fiber type disproportion (CFTD) · *DMPK* · CTG expansion · *ACTA1* · *TPM3*

Introduction

Congenital myotonic dystrophy (CDM; OMIM 160900) is caused by marked expansion of trinucleotide (CTG) repeat in the 3′ untranslated region of the dystrophia myotonica protein kinase gene (*DMPK*; OMIM 605377) on chromosome 19q [1, 5, 9]. The CTG repeat in normal individuals varies from 5 to 35, whereas it expands to more than 1,000 repeats in CDM [7]. Typically, the mothers of CDM patients show clinical features of myotonic dystrophy which makes the diagnosis of CDM easier. Clinically, CDM patients show hypotrophy at birth, tented upper lip, facial muscle weakness, and neonatal respiratory insufficiency. Mental retardation becomes evident in later life. On muscle pathology, the presence of numerous immature fibers with peripheral halo is a characteristic feature together with increased number of fibers with centrally placed nuclei and hypotrophy of type 1 fibers, mimicking myotubular myopathy [6].

Smaller sized type 1 fibers as compared to type 2 fibers are a characteristic pathological feature of congenital fiber type disproportion (CFTD; OMIM 255310). CFTD is a

Electronic supplementary material The online version of this article (doi:10.1007/s00401-010-0660-7) contains supplementary material, which is available to authorized users.

K. Tominaga · Y. K. Hayashi · K. Goto · N. Minami · S. Noguchi · I. Nonaka · I. Nishino (✉)
Department of Neuromuscular Research, National Institute of Neuroscience, National Center of Neurology and Psychiatry, 4-1-1 Ogawa-higashi, Kodaira, Tokyo 187-8502, Japan
e-mail: nishino@ncnp.go.jp

T. Miki
Proteo-Medicine Research Center, Ehime University, Toon, Ehime 791-0295, Japan

K. Tominaga · T. Miki
Department of Geriatric Medicine, Ehime University Graduate School of Medicine, Toon, Ehime 791-0295, Japan

congenital myopathy defined by type 1 fiber hypotrophy of 12% or more than type 2 fibers, and with the absence of structural abnormalities within myofibers [2]. Type 1 fiber predominance is also commonly seen. Clinically, CFTD patients show hypotonia, facial muscle weakness, and severe respiratory insufficiency at birth. Long face, high-arched palate, and joint contractures are often seen. CFTD is a genetically heterogeneous disorder and mutations in the genes for tropomyosin 3 (*TPM3*; OMIM 191030), α-skeletal muscle actin 1 (*ACTA1*; OMIM 102610), and selenoprotein N1 (*SEPN1*; OMIM 606210) have been identified [3, 4, 8]. Reportedly *TPM3* mutations are the most common ones and observed approximately in 20–25% of the CFTD patients [4]. *ACTA1* mutations were identified in 6% of CFTD [8], and only one family was reported having an *SEPN1* mutation [3].

Although the muscle pathology features of CDM seem to be well defined, our experience with one CDM patient who was previously diagnosed as CFTD made us hypothesize that CDM may have features other than the presently defined ones, both in terms of muscle pathology and clinical characteristics. In this study, we looked for CDM patients among patients who presented with CFTD. We also performed clinical and pathological analysis to find out whether patients with CDM can be distinguished from CFTD.

Materials and methods

Patients

All clinical materials used in this study were obtained for diagnostic purposes and with informed consent. This work was approved by the Ethical Committee of National Center of Neurology and Psychiatry (NCNP). In this study, we chose muscle specimens from patients younger than 1 year of age. From the muscle repository of NCNP, there were 28 unrelated patients who were pathologically diagnosed as CFTD. Twenty CDM patients, who had symptomatic family members and whose diagnosis was genetically confirmed, were also used for comparison.

Histochemistry

Biopsied skeletal muscles were frozen with isopentane cooled in liquid nitrogen. Serial frozen sections of 10 μm thickness were stained with hematoxylin and eosin (H & E), modified Gomori-trichrome (mGT), NADH-tetrazolium reductase (NADH-TR), and ATPases (pH 10.6, pH 4.6 and pH 4.3). For each muscle specimen, the mean fiber diameter was determined by obtaining the shortest anteroposterior diameter of 100 each of type 1 and type 2 (A + B) fibers using ATPase stains. The myofiber diameter was used to calculate the fiber size disproportion (FSD). FSD was computed as: difference of type 2 fiber diameter (mean) and type 1 fiber diameter (mean) divided by type 2 fiber diameter (mean) × 100%.

Genetic analyses

Genomic DNA was extracted from peripheral lymphocytes or frozen muscle specimens using standard protocol. To examine CTG repeat expansion in *DMPK*, triplet repeat primed PCR was performed as described previously [12]. The presence of the expanded CTG repeats was examined by Gene Mapper using ABI PRISM 310 automated sequencer (Applied Biosystems Japan Co., Ltd, Japan). To know the approximate number of triplet repeats, we performed Southern blotting analysis using PCR-amplified CTG repeats because of the limited amounts of muscle specimens [10]. The primer sequences used in this study are F: 5′-CGAACGGGGCTCGAAGGGTCCTTGTAGC CG-3′, and R: 5′-TCTTTCTTTACCAGACACTAGGG-3′.

The PCR products were electrophoresed with 1% of Seakem HGT agarose gel (Cambrex Bio Science Rockland Inc., ME, USA), transferred to Hybond-XL (GE Healthcare, UK) for overnight, hybridized with ^{32}P-labeled probes of $(CTG)_{10}$ oligonucleotide at 65°C for overnight, and detected using BAS2500 (Fuji Film, Japan). By using genomic DNA from a CDM patient with known CTG repeat number, we confirmed that this PCR-based method can detect the corresponding size of the CTG repeats using genomic DNA. For mutation screening of *ACTA1* and *TPM3*, all exons and their flanking intronic regions were amplified by PCR and directly sequenced by an ABI PRISM 3100 automated sequencer (Applied Biosystems). Primer sequences are listed in the Supplemental Table.

Statistical analyses

All data are presented as means ± SD. Comparisons among groups were done by using Student's *t* test and analysis of variance (ANOVA) as appropriate. Statistical significance was considered when p value was less than 0.05.

Results

Genetic analyses

By using triplet repeat primed PCR, expanded CTG repeats in *DMPK* were detected in 4 of 28 (14%) unrelated patients who were pathologically diagnosed as CFTD (Figs. 1, 2a). This diagnosis of CDM was further confirmed by Southern

blotting analysis, wherein all four patients had more than 1,000 CTG repeats (Fig. 2b). We also identified three heterozygous *ACTA1* mutations (p.Gly48Cys, p.Leu221-Pro, and p.Pro332Ser) in four unrelated CFTD patients. Two mutations of p.Leu221Pro and p.Pro332Ser have already been reported [8], whereas the p.Gly48Cys mutation observed in two patients was a novel one. The Gly48 is a highly conserved amino acid among several species. Two unrelated CFTD patients had the same heterozygous mutation p.Arg168Cys in *TPM3*, which was previously reported in CFTD patients [4].

Clinical findings

We compared the clinical findings among 4 CFTD patients with CTG expansion and 6 CFTD patients with *ACTA1* or *TPM3* mutations, and compared the clinical features with 20 patients genetically confirmed as CDM (Table 1). In terms of family history, none of the four CFTD patients with CTG expansion had a positive family history. This is in stark contrast with the typical picture in CDM patients, as all of them had at least one symptomatic family member. Hydramnios and premature delivery were seen in more than 50% of the CFTD patients with CTG expansion and CDM, but none of CFTD patients with *ACTA1* or *TPM3* mutations. Hypotonia and respiratory insufficiency at birth were seen in all groups except for two patients with *TPM3* mutation.

Muscle pathological findings

As muscle pathology can have drastic changes according to the gestational age of infantile patients, we adjusted the age by setting the full-term day (37 weeks of gestation) as putative birthday. After adjustment, the age at biopsy of the CDM patients ranged from −7 to 43 weeks, and those of the four CFTD patients with CTG expansion were from 21 to 42 weeks.

Congenital fiber type disproportion is defined as a congenital myopathy wherein FSD is higher than 12%, but with no associated structural abnormalities within the myofibers [2]. In this study, FSD in CDM, CFTD with CTG expansion, CFTD with *ACTA1* mutation, and CFTD with *TPM3* mutation was calculated to be 7.2 ± 6.8% (mean ± SD), 23.0 ± 5.0, 47.5 ± 4.0, and 52.0 ± 9.9%, respectively (Fig. 3). FSD was significantly ($p < 0.05$) higher in CFTD with *ACTA1* or *TPM3* mutations as compared to the CFTD patients with CTG expansion and CDM.

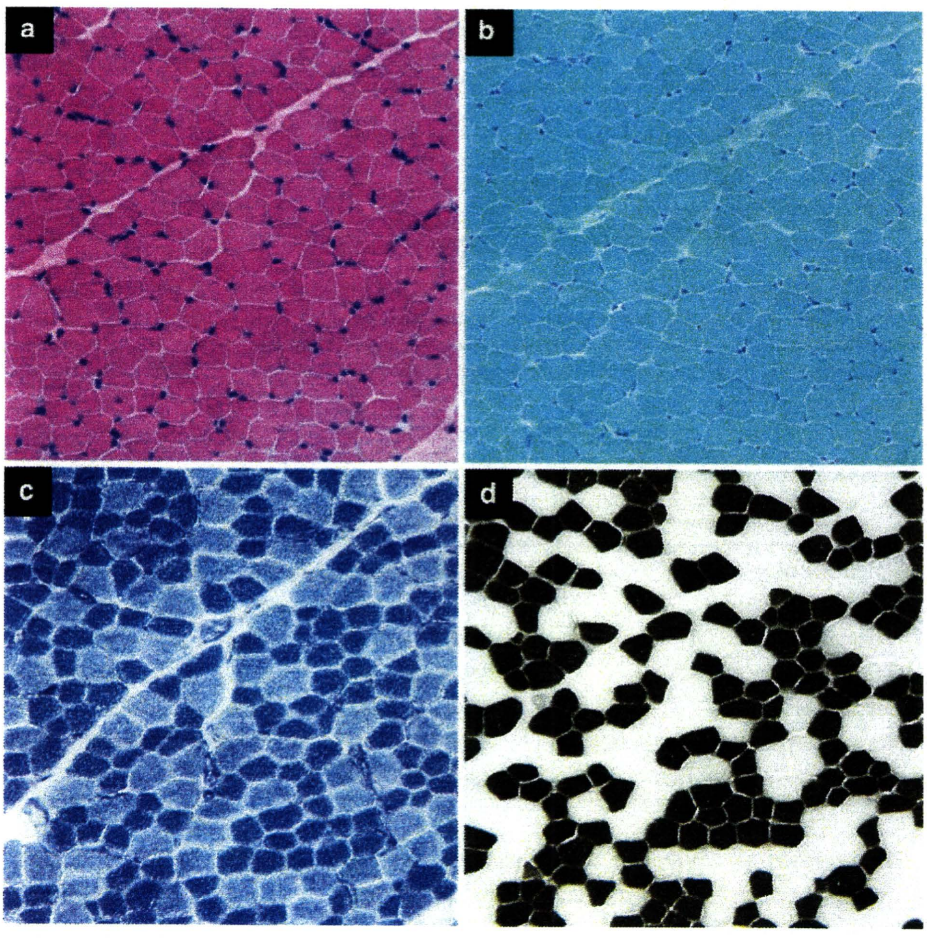

Fig. 1 Muscle pathology of a 42-week-old CFTD patient with CTG expansion. **a** Hematoxylin and eosin, **b** modified Gomori trichrome, **c** NADH-TR, and **d** ATPase (pH 4.4) stain. Type 1 fiber atrophy (FSD [(mean type 2 fiber diameter) − (mean type 1 fiber diameter)/mean type 2 fiber diameter × 100] = 26%), type 1 fiber predominance (65%), and only 1% of type 2C fibers with no peripheral halo is seen. *Bar* 50 μm

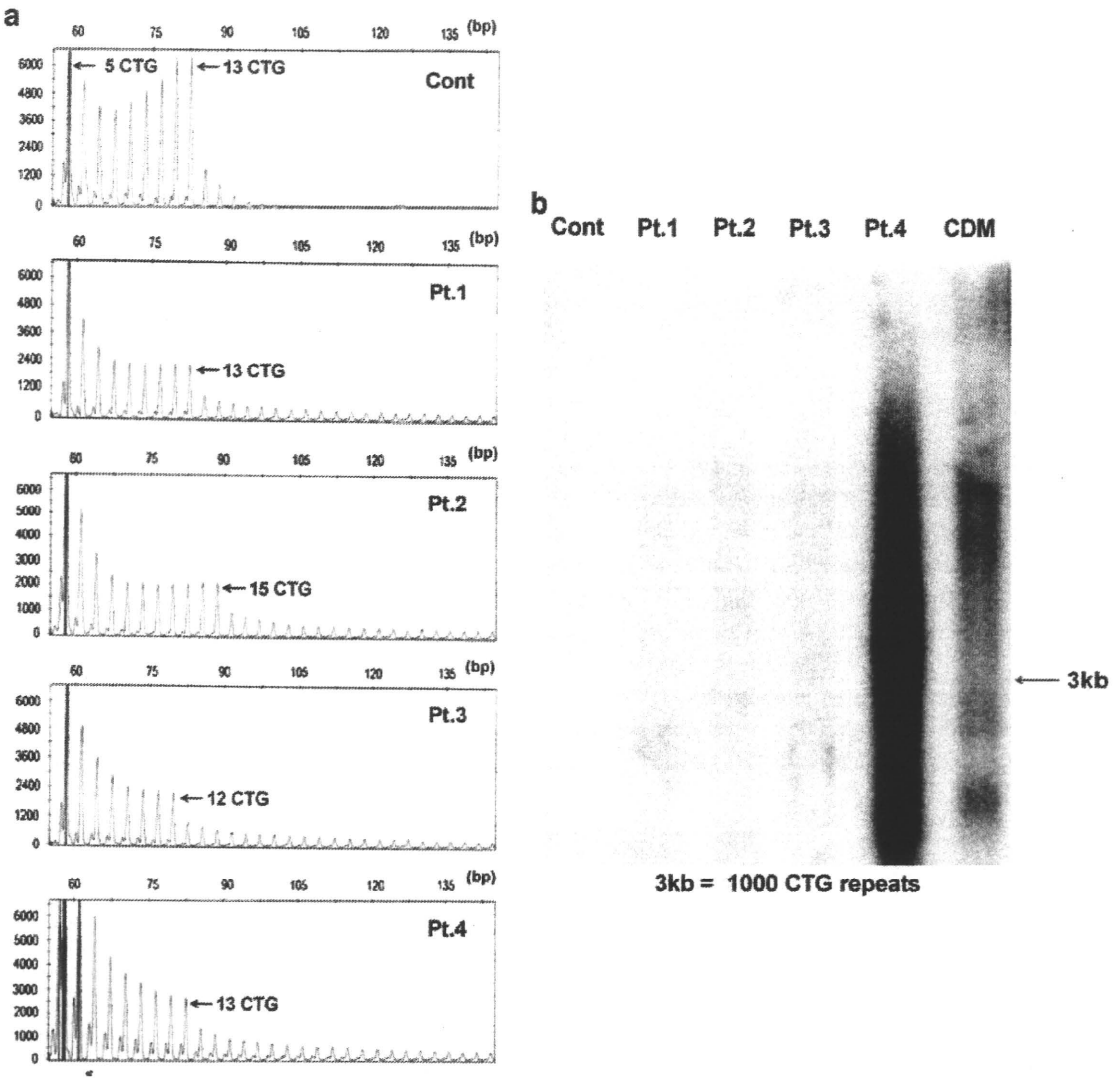

Fig. 2 Genetic analyses. **a** Triplet repeat primed PCR. Control (*Cont*) has 5 and 13 CTG repeats. The four CFTD patients (Pt.1, Pt.2, Pt.3, and Pt.4) have the ladder pattern that represents a large CTG allele together with higher peaks that show normal-sized allele (*arrows*). **b** Southern blotting analysis using PCR products. Four CFTD patients (Pt.1, Pt.2, Pt.3, and Pt.4) and one genetically confirmed CDM showed smear band larger than 3 kb corresponding to 1,000 CTG repeats, whereas a control (*Cont*) has no detectable band

Table 1 Clinical summary of the patients

Pathological diagnosis	CDM	CFTD	CFTD	CFTD
Gene mutation	CTG expansions in *DMPK*	CTG expansions in *DMPK*	*ACTA1*	*TPM3*
Number of patients	20	4	4	2
Hydramnios	65% (13/20)	50% (2/4)	0% (0/4)	0% (0/2)
Premature delivery (<37w)	50% (10/20)	50% (2/4)	0% (0/4)	0% (0/2)
Hypotonia at birth	100% (20/20)	100% (4/4)	100% (4/4)	0% (0/2)
Respiratory insufficiency at birth	95% (19/20)	75% (3/4)	75% (3/4)	0% (0/2)
Symptoms seen in family	100% (20/20)	0% (0/4)	0% (0/4)	0% (0/2)

In addition to FSD, we also checked other features in pathology that define either CFTD or CDM. Type 1 fiber predominance is a notable pathological finding observed in CFTD, and all our CFTD patients, including those with CTG expansion, showed type 1 fiber predominance. The mean composition of type 1 fibers in CDM, CFTD with

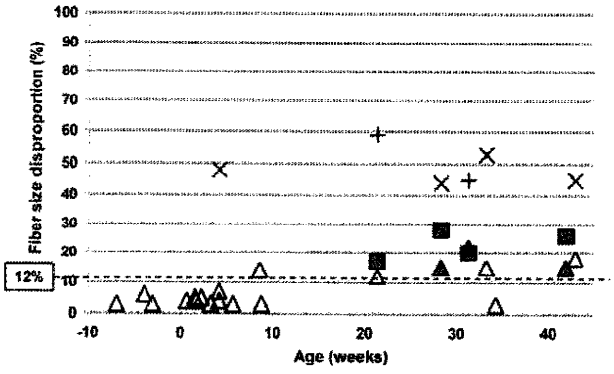

Fig. 3 Fiber size disproportion (*FSD*) of each patient. CFTD with CTG expansion (*filled square*; $N = 4$), CDM (*open triangle*; $N = 17$), CDM with similar pathological findings to CFTD (*filled triangle*; $N = 3$), CFTD with *ACTA1* mutations (*multi symbol*; N = 4), and CFTD with *TPM3* mutations (*plus*; $N = 2$). *Dot line* at 12% of FSD is the lowest FSD by the definition of CFTD

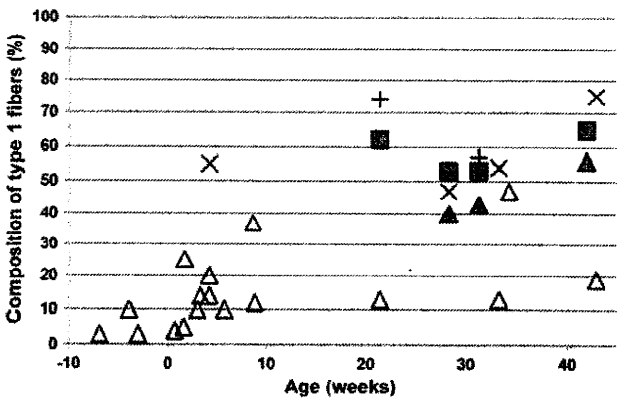

Fig. 4 Composition of type 1 fibers in each patient. *Filled square* CFTD with CTG expansion, *open triangle* CDM, *filled triangle* CDM with similar pathological findings to CFTD, *multi symbol* CFTD with *ACTA1* mutations, and *plus* CFTD with *TPM3* mutations

CTG expansion, and CFTD with *ACTA1* or *TPM3* mutations was 19.6 ± 16.3, 58.2 ± 6.2, 57.8 ± 2.0, and 65.5 ± 12.0%, respectively (Fig. 4). On the other hand, the presence of numerous immature type 2C fibers with peripheral halo is a characteristic finding in CDM. A markedly increased number of type 2C fibers were actually observed in CDM especially in patients younger than 10 weeks of adjusted age (Fig. 5). The frequency of type 2C fibers was inversely correlated to age of patients, while the number of type 1 fibers was directly proportional to age of patients. In other words, type 2C fibers were increased among younger age, while type 1 fiber predominance is seen more among older patients. Peripheral halo was observed in 14 of 20 (70%) CDM patients even in a 43-week-old patient. In CFTD patients with CTG expansion, type 2C fibers accounted for less than 20% and in CFTD with *ACTA1* or *TPM3* mutations, only a few type 2C fibers were seen. No peripheral halo was seen in either group. The increased number of fibers with internally located nuclei is another characteristic pathological finding of myotonic dystrophy. In our series, fibers containing internal nuclei were variably increased up to 26% in CDM patients, whereas less than 2% of fibers contained internal nuclei in the CFTD patients with CTG expansion or mutation in *ACTA1* or *TPM3*. The number of the fibers with internal nuclei is relatively correlated to the number of immature fibers in CDM, which may reflect immaturity of the fibers as described previously [6, 11].

Of the 20 CDM patients, 3 showed pathological findings similar to CFTD with CTG expansion. The ages of these three patients were 29, 32 and 42 weeks, respectively. FSD was 15–21%, with less than 20% of type 2C fibers and no peripheral halo. In these patients, the clinical diagnosis of CDM was made based upon the presence of the symptomatic family member.

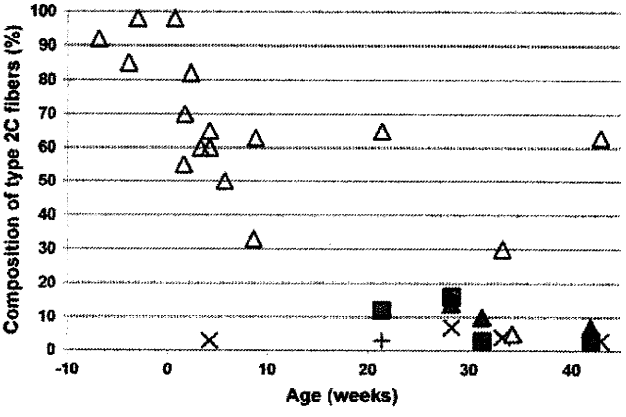

Fig. 5 Composition of type 2C fibers in each patient. *Filled square* CFTD with CTG expansion, *open triangle* CDM, *filled triangle* CDM with similar pathological findings to CFTD, *multi symbol* CFTD with *ACTA1* mutations, and *plus* CFTD with *TPM3* mutations

Discussion

In this study, we identified 4 of 28 patients (14%) who have CTG expansion in *DMPK* but were pathologically diagnosed as CFTD. Clinical symptoms of CFTD and CDM are quite similar during neonatal stage, including hypotonia and respiratory insufficiency. However, most of CDM patients are readily diagnosed by the presence of symptomatic family members, typically the mother. In fact, all CDM patients in our series had symptomatic family members and 75% of the mothers had the diagnosis of myotonic dystrophy. In contrast, no notable clinical symptoms were recorded in the mother of the CFTD patients with CTG expansion, and we could not examine the repeat size of the mothers. No marked difference in the size of CTG repeats was seen between CFTD patients with CTG expansion and CDM.

Among the CDM patients we examined, three patients showed pathological findings similar to those observed in CFTD with CTG expansion. They showed a small number of type 2C fibers, no peripheral halo, and hypotrophy of type 1 fibers (FSD >15%). The diagnosis of CDM was done from the typical clinical symptoms of myotonic dystrophy observed in the family member. Interestingly the ages of these three patients were over 29 weeks. Consistently, the ages of the patients who have CFTD with CTG expansion ranged from 21 to 42 weeks. These results suggest that CFTD pathology may be seen in this age range of CDM patients.

We identified four patients with mutations in *ACTA1* and two in *TPM3*. FSD in these patients was over 45% and significantly higher than that observed in CFTD with CTG expansion. This finding is also consistent with a previous report of CFTD patients with *TPM3* mutations whose muscle showed higher than 50% of FSD [4]. From these results, CDM should be considered for the patients whose muscle shows CFTD with FSD lower than 40%. In our series, only 4 (14%) and 2 (7%) of 28 patients had the mutations respectively in *ACTA1* and *TPM3*, leaving 18 (65%) patients still genetically uncharacterized and suggesting that defects in these genes may not be the major causes of CFTD in Japan. Further studies are necessary to elucidate such causes.

Acknowledgments We thank Dr. May Christine V. Malicdan (National Institute of Neuroscience, NCNP) for reviewing the manuscript. This study was supported by: the a Grant-in-Aid for Scientific Research and a Grain-in-aid for Exploratory Research from Japan Society for the Promotion of Science; by Research on Psychiatric and Neurological Diseases and Mental Health of Health Labour Sciences Research Grant and the Research Grant (20B-12, 20B-13) for Nervous and Mental Disorders from the Ministry of Health, Labour, and Welfare; by Research on Health Sciences focusing on Drug Innovation from the Japanese Health Sciences Foundation; and by the Program for Promotion of Fundamental Studies in Health Sciences of the National Institute of Biomedical Innovation (NIBIO).

References

1. Brook JD, McCurrach ME, Harley HG et al (1992) Molecular basis of myotonic dystrophy: expansion of a trinucleotide (CTG) repeat at the 3′ end of a transcript encoding a protein kinase family member. Cell 69:385
2. Clarke NF, North KN (2003) Congenital fiber type disproportion—30 years on. J Neuropathol Exp Neurol 62:977–989
3. Clarke NF, Kidson W, Quijano-Roy S et al (2006) SEPN1: associated with congenital fiber-type disproportion and insulin resistance. Ann Neurol 59:546–552
4. Clarke NF, Kolski H, Dye DE et al (2008) Mutations in TPM3 are a common cause of congenital fiber type disproportion. Ann Neurol 63:329–337
5. Fu YH, Pizzuti A, Fenwick RG Jr et al (1992) An unstable triplet repeat in a gene related to myotonic muscular dystrophy. Science 255:1256–1258
6. Harper PS, Monckton DG (2004) Myotonic dystrophy. In: Engel AG, Franzini-Armstrong C (eds) Myology, 3rd edn. McGraw-Hill, New York, pp 1039–1076
7. The International Myotonic Dystrophy Consortium (IDMC) (2000) New nomenclature and DNA testing guidelines for myotonic dystrophy type 1 (DM1). Neurology 54:1218–1221
8. Laing NG, Clarke NF, Dye DE et al (2004) Actin mutations are one cause of congenital fibre type disproportion. Ann Neurol 56:689–694
9. Mahadevan M, Tsilfidis C, Sabourin L et al (1992) Myotonic dystrophy mutation: an unstable CTG repeat in the 3′ untranslated region of the gene. Science 255:1253–1255
10. Surh LC, Mahadevan M, Korneluk RG (1998) Analysis of trinucleotide repeats in myotonic dystrophy. In: Dracopoli NC, Haines JL, Korf BR, Morton CC et al (eds) Current protocols in human genetics, vol 2. Wiley, New York, unit 9.6.1-13
11. Tanabe Y, Nonaka I (1987) Congenital myotonic dystrophy. Changes in muscle pathology with ageing. J Neurol Sci 77:59–68
12. Warner JP, Barron LH, Goudie D et al (1996) A general method for the detection of large CAG repeat expansions by fluorescent PCR. J Med Genet 33:1022–1026

Mechanisms of Genomic Instabilities Underlying Two Common Fragile-Site-Associated Loci, *PARK2* and *DMD*, in Germ Cell and Cancer Cell Lines

Jun Mitsui,[1] Yuji Takahashi,[1] Jun Goto,[1] Hiroyuki Tomiyama,[2] Shunpei Ishikawa,[3] Hiroyo Yoshino,[4] Narihiro Minami,[5] David I. Smith,[6] Suzanne Lesage,[7] Hiroyuki Aburatani,[8] Ichizo Nishino,[5] Alexis Brice,[7] Nobutaka Hattori,[2] and Shoji Tsuji[1,*]

Common fragile sites (CFSs) are specific chromosome regions that exhibit an increased frequency of breaks when cells are exposed to a DNA-replication inhibitor such as aphidicolin. *PARK2* and *DMD*, the causative genes for autosomal-recessive juvenile Parkinsonism and Duchenne and Becker muscular dystrophy, respectively, are two very large genes that are located within aphidicolin-induced CFSs. Gross rearrangements within these two genes are frequently observed as the causative mutations for these diseases, and similar alterations within the large fragile sites that surround these genes are frequently observed in cancer cells. To elucidate the molecular mechanisms underlying this fragility, we performed a custom-designed high-density comparative genomic hybridization analysis to determine the junction sequences of approximately 500 breakpoints in germ cell lines and cancer cell lines involving *PARK2* or *DMD*. The sequence signatures where these breakpoints occur share some similar features both in germ cell lines and in cancer cell lines. Detailed analyses of these structures revealed that microhomologies are predominantly involved in rearrangement processes. Furthermore, breakpoint-clustering regions coincide with the latest-replicating region and with large nuclear-lamina-associated domains and are flanked by the highest-flexibility peaks and R/G band boundaries, suggesting that factors affecting replication timing collectively contribute to the vulnerability for rearrangement in both germ cell and somatic cell lines.

Introduction

Common fragile sites (CFSs) are specific chromosome regions that exhibit an increased frequency of gaps or breaks when cells are exposed to a DNA replication inhibitor such as aphidicolin. CFSs are well known to be predisposed to breakages and rearrangements, particularly in cancer cells. Recently, it was reported that aphidicolin-mediated replication stress could induce large submicroscopic deletions at CFSs in a human-mouse cell-hybrid system.[1] Many of the aphidicolin-induced CFSs have been found to span extremely large genes, including *PARK2* (MIM 602544), *DMD* (MIM 300377), *FHIT* (MIM 601153), *WWOX* (MIM 605131), *GRID2* (MIM 602368), *LARGE* (MIM 603590), *CTNNA3* (MIM 607667), *NBEA* (MIM 604889), and *CNTNAP2* (MIM 604569).[2] Intriguingly, *PARK2* and *DMD* are both genes responsible for human hereditary diseases, and gross deletions are frequently observed as the causative germline mutations.

PARK2 (chromosome 6: 161,688,580–163,068,824, NCBI build 36.1), encompassing 1.4 Mb, which is embedded in a CFS (FRA6E), is the gene responsible for autosomal-recessive juvenile Parkinsonism (AR-JP [MIM 600116]).[3] Among various causative germline mutations in *PARK2*, gross deletions account for 50 to 60% of causative germline mutations,[4] with the deletion hotspots clustering in exons 3 and 4.[5] As the consequence of the localization of *PARK2* in FRA6E, *PARK2* is also frequently targeted by deletions in various cancer cells.[6] *DMD* (chromosome X: 31,047,266–33,139,594), which is also embedded in a CFS (FRAXC),[7] encompasses 2.1 Mb and is the gene responsible for Duchenne and Becker muscular dystrophy (DMD and BMD [MIM 310200 and 300376]).[8] Similarly to *PARK2*, *DMD* is also frequently targeted by gross deletions in patients with DMD or BMD (hereafter DMD/BMD) and in those with various cancers.[7,9] Approximately 60% of causative germline mutations are gross deletions, and deletion hotspots are in exons 45 to 52.[10] Although it has not drawn much attention, the frequent occurrence of gross rearrangements in the genomic regions corresponding to CFSs in patients with AR-JP or DMD/BMD suggests that a common basis underlies the frequent occurrence of rearrangements in both germ cell and somatic cell lines. CFSs are chromosomal regions that are particularly sensitive to certain forms of replication stress, and there are lines of evidence suggesting that CFSs represent unreplicated DNA resulting from stalled replication forks.[11,12] These sites replicate late during the S phase, even under normal culture conditions.[13,14] The context of the nucleotide sequences and/or chromosomal structures at these CFSs leading to delay replication,

[1]Department of Neurology, Graduate School of Medicine, University of Tokyo, Tokyo 113-8655, Japan; [2]Department of Neurology, Juntendo University School of Medicine, Tokyo 113-8421, Japan; [3]Department of Pathology, Graduate School of Medicine, University of Tokyo, Tokyo 113-8655, Japan; [4]Research Institute for Diseases of Old Ages, Juntendo University School of Medicine, Tokyo 113-8421, Japan; [5]Department of Neuromuscular Research, National Institute of Neuroscience, National Center of Neurology and Psychiatry, Tokyo 187-8502, Japan; [6]Division of Experimental Pathology, Department of Laboratory Medicine and Pathology, Mayo Clinic College of Medicine, Rochester, MN 55902, USA; [7]CRicm, University Pierre et Marie Curie, INSERM, UMR_S975, CNRS UMR 7225, Hospital Pitié-Salpêtrière, 75651 Paris, CEDEX 13, France; [8]Genome Science Division, Research Center for Advanced Science and Technology, University of Tokyo, Tokyo 153-8904, Japan
*Correspondence: tsuji@m.u-tokyo.ac.jp
DOI 10.1016/j.ajhg.2010.06.006.